High quality factor, protein-based microlasers from self-assembled microcracks

Tam Trong Nguyen[1], Hanh Hong Mai[1], Thin Van Pham[2], Thau Xuan Nguyen[2] and Van Duong Ta[3,*]

[1] Department of Quantum Optics, Faculty of Physics, University of Science, Vietnam National University, 334 Nguyen Trai, Hanoi 100000, Vietnam
[2] Department of Physics, Le Quy Don Technical University, 236 Hoang Quoc Viet, Hanoi 100000, Vietnam
[3] Department of Optical Devices, Le Quy Don Technical University, 236 Hoang Quoc Viet, Hanoi 100000, Vietnam

*E-mail: duong.ta@mta.edu.vn

Received xxxxxx
Accepted for publication xxxxxx
Published xxxxxx

Abstract

In the last decade, microbiolasers made of biological materials have shown their great prospect in biosensing and bioimaging. Several types of confinement including Fabry-Pérot, distributed feedback, whispering gallery mode cavities have been employed for microbiolasers. However, these lasers need to have an optimized design for obtaining resonant feedback and their operation is strongly affected by a cavity defect. In this work, we demonstrate protein-based microcrack lasers that can operate with random shapes. They are fabricated by a fast, one-step self-assembled process. A lasing threshold of 13.6 mJ/cm^2 and quality (Q) factor up to around 3×10^3 are achieved. These values are comparable with biolasers that rely on conventional cavities. Interestingly, we have found that the common whispering gallery mode lasing also can be realized from a microcrack with a nonsymmetrical structure. This result opens a new possibility for making microlasers with excellent properties. Owing to simple fabrication, high Q factor, low lasing threshold and biocompatibility, these microcrack biolasers have the potential for integrated photonic circuits and biosensing applications.

Keywords: biolasers, microlasers, crack, protein

1. Introduction

Recently, biolasers has been attracted a lot of attention due to their biocompatibility and excellent optical properties [1]. Generally, a biolaser can be achieved by using a biomaterial cavity doped with an organic dye serving as a gain medium [2–4]. In some cases, the biomaterial itself can provide emission for the laser [5–7]. Biolasers have many applications in biosensing [7,8] and bio-imaging [9–11]. Furthermore, thanks to the biocompatibility and small sizes, micro-biolasers can be integrated into single cells for cell-tagging and cell-tracking without causing any damage to the living samples [12–15].

Many efforts have been made to achieve biological microlasers by using various cavity structures such as Fabry-Pérot (FP) [16,17], distributed feedback (DFB) [18], Whispering gallery mode (WGM) [19–21] and random cavities [22–24]. The conventional architectures such as FP, DFB and WGM have shown their great advantages in making high quality (Q) factor miniaturized biolasers. However, these lasers need to have an optimized design for obtaining resonant feedback and their operation is strongly affected by a cavity defect. Random microlasers, on other hand, less effected by structure defect because they rely on multiple scattering to amplify light [25]. As a result, it would be great if there is a type of laser that offers high Q factor comparable with

 © xxxx IOP Publishing Ltd

conventional lasers but also can operate with any random shapes like random lasers.

It has been demonstrated that self-assembled crack can be useful in making micro and nanostructures [26]. Lately, these microstructures have been demonstrated as an excellent medium for random laser generation [27,28]. In these researches, a system of crack structures was investigated thus the lasing mechanism is very complex. The use of a single microcrack, especially from biomaterial, for a miniaturized laser has not been explored. In this work, we show that protein-based microlasers with high Q factor can be achieved from self-assembled microcracks using one-step and cost-effective fabrication process.

2. Materials and methods

2.1. Preparing for dye-doped protein solution

Bovine serum albumin (BSA, ≥98% purity) was purchased from Bio-Basics and Rhodamine B (RhB, ≥95% purity) was purchased from Sigma-Aldrich. Dye-doped BSA solution was prepared by mixing a 2 mL BSA aqueous solution (25 wt%) and 0.5 mL RhB solution (0.5 wt%).

2.2. *Fabrication of protein-based microcrack lasers*

Microcrack lasers were fabricated by a simple drop-casting method. A drop of dye-doped BSA solution was deposited on a glass substrate and subsequently heated at a constant temperature of 70^{o}C for around 4 minutes. Due to the heat generation, water is evaporated and a dye-doped thin film is formed. In the end, crack patterns were self-assembly created in the film due to residual stress. The dry mass ratio of BSA and RhB are around 99.5% and 0.5%, respectively.

2.3. Optical characterizations

Optical properties of protein-based microcrack lasers were investigated by micro-photoluminescence (μ-PL) setup. The samples were optically pumped by a focused laser beam of 532 nm from a Nd:YAG nanosecond pulse laser (Litron Lasers) with a repetition rate of 10 Hz and a pulse duration of 7 ns. A system consists of a microscope with a 10X objective lens and a spectrometer (AvaSpec-2048L) was used to collect and record photoluminescence (PL) emission from the sample. The spectral resolution is ~0.2 nm.

3. Results and discussion

3.1 Self-assembled microstructure via cracks

Fig. 1 (a) demonstrates the formation of crack structures on a drying droplet of dye-dope BSA solution. During the heating process, the droplet dries from the edge to the centre. As the contact region remains stationary, the increase of tensile stress forms cracks at defective regions (fragile regions) [29]. At t = 60 s, crack lines begin to appear radially and then propagate in random directions. In the next 100 s, water completely evaporates and many crack patterns are formed. The crack patterns can be seen more clearly in a SEM image (fig. 1 (b)). The cracks appear with sharp and smooth edges which can be served as reflectors for the lasing generation (fig. 1 (c)). The thickness of the crack is around 10 μm.

3.2 Lasing emission from a crack structure

Under optical pumping, protein-based crack structures can operate as random lasers with a relatively low threshold and high Q-factor. Fig. 2 (a) demonstrates the PL spectra of a crack structure under increasing pump pulse fluence (PPF). For the excitation of 13.6 mJ/cm^2, the PL signals exhibit broad and low intensity spectrum which is the characteristic of spontaneous emission. When the PPF reaches 23.8 mJ/cm^2, sharp peaks start to appear with significantly higher intensity compared with the spontaneous emission background.

The change of PL intensity as a function of PPF is shown in fig. 2 (b). The integrated intensity initially increases linearly with the increase of PPF before a sudden rise is observed at 18.0 mJ/cm^2 which is indicated the lasing threshold.

It is suggested that light travels horizontally in crack structures. When the light is headed to the sidewalls, part of it is scattered out (bright emission can be seen from edges of cracks as shown in the inset of Fig. 2) while the rest is reflected. This process happens many times and the reflected light provides necessary resonant feedback for lasing emission. As the edges are not parallel, the feedback mechanism does not like FP cavity but more complex. As a result, this laser is classified as a random laser [27].

In this work, in order to make microlasers, we focus on studying single micron-sized structures.

3.3 Lasing emission from a single microcrack

The lasing properties of a microcrack were investigated by optically pumping at different positions as shown in fig. 3 (a). The length at the middle of the pumped region is *L*. This value is proportional to the pumped area on the sample. It was found the lasing threshold value increases with the decrease of pumped area (fig. 3 (b)). The lasing threshold increases by approximately 2.5 times when the mean length decreases 2 times, from 82 μm (position A) to 42 μm (position D). The inverse relationship between pump area and threshold can be explained by the fact that a larger pump area means more dye molecules are excited thus stimulated amplification can be achieved more easily. Similar phenomena have been observed experimentally in other researches on WGM micro-biolasers [23,30,31].

Fig. 3 (c) demonstrates the PL spectrum above the lasing threshold of different pumped positions with descending *L*. The lasing emission blue-shifted (about 5 nm) with decreasing

L which can be explained by many reasons including confinement effect and reabsorption of the gain medium [32].

Understanding the lasing mechanism is an essential aspect of any laser study. Herein, it is suggested that the sidewalls of the micro-crack can be served as reflectors for the optical feedback that leads to lasing action. The cavity feedback can be determined by studying the free spectral range (FSR) of the lasing spectrum. At positions A, B and C, the FSR of lasing spectra are not clear therefore it is hard to determine exactly the optical path. However, at position D, lasing mode exhibit a clear spacing and FSR is measured to be around 1.7 nm. As a result, it is possible to find out the feedback mechanism and this will be studied in detail in the next section.

3.3 Whispering gallery mode lasing emission from a single microcrack.

We have investigated the lasing mechanism at position D of the microcrack (as shown in fig. 3 (a)). Three possible optical paths can support optical feedback (fig. 4 (a)). Based on the FSR, the cavity length can be calculated as $L = \lambda_m^2/(n \cdot FSR)$, where λ_m is the lasing wavelength, n is the refractive index of the cavity a. Assuming $\lambda_m = 616.4\,nm$, the calculated cavity length is $L = 153\,\mu m$. This value is far different compared with the optical path of the case 1 ($2 \cdot L_{D1} = 575\,\mu m$) and case 2 ($2 \cdot L_{D2} = 88\,\mu m$). Therefore, the FP cavity is not reasonable for the lasing action. However, for case 3, the optical path length of the WGM-like cavity is $L_{D3} = 154\,\mu m$ which is consistent with the above calculated value ($L = 153\,\mu m$). As a result, we suggest that WGM is the feedback mechanism for the lasing action at the position D. This is a very interesting result as WGM lasing is generally obtained from highly symmetric structures like microspheres, microdisks [30,33].

As WGM supports the lasing action, lasing modes can be calculated by the equation $m = nL/\lambda_m$ (m is the mode number). We found m = 361-373 that shows good agreement with the obtained lasing spectrum (fig. 4 (b)). Owing to low optical loss, WGM lasing generally provides a high Q factor. The Q factor has been determined to be 2800 ($Q = \lambda/\Delta\lambda$) which is comparable with the lasing achieved by conventional WGM microlasers [8,21]

3.5 Lasing emission from different microcracks

It is exciting to find that the protein-based microcracks can lase in any random shapes. Fig. 5 demonstrates the PL emission spectrum of the microcracks and their corresponding integrated intensity as a function of PPF. The lasing emission of the 150 µm crack appears from 615 nm to 640 nm (fig. 5 (a)) with a lasing threshold of 14.3 mJ/cm^2 (fig. 5 (b)). The emission range of the 50 µm crack is between 595 nm and 607 nm (fig. 5 (c)), a slight blue-shift compared with the 150 µm. Due to smaller size, the lasing threshold of the 50 µm crack is 26.4 mJ/cm^2, about 2 time higher compared with the 150 µm crack laser. This result is consistent with the lasing characteristics of the long microcrack discussed in section 3.2.

The full width at half maximum (FWHM) of a lasing mode is determined to be 0.22 nm at 638.62 nm for the 150 µm crack laser indicating rather high Q-factor of 2900. This value is comparable or even higher compared with starch-based microlasers [8] and silk-based microlasers [30] whose the fabrication processes were much more complicated.

4. Conclusions

We have demonstrated that the dye-doped protein-based microcracks are an excellent candidate for biological microlasers. The microcracks can be obtained by a simple and fast (several minutes) self-assembled process. Lasing with a high Q factor of around 3×10^3 can be achieved from microstructures with random shapes. Interestingly, we have found that WGM lasing can be obtained from a nonsymmetrical microcrack which opens a new possibility for making microlasers with excellent properties. As these microcrack biolasers rely on a simple fabrication technique but can provide high Q factor, low lasing threshold they are promising for real applications in biosensing and bioimaging.

Acknowledgements

This research is funded by Vietnam National Foundation for Science and Technology Development (NAFOSTED) under grant number 103.03-2017.318. Mr Tam Trong Nguyen thanks the Domestic Master Scholarship Programme of Vingroup Innovation Foundation, code: VINIF.2020.ThS.67.

References

[1] Chen Y C and Fan X 2019 Biological Lasers for Biomedical Applications *Adv. Opt. Mater.* **7** 1–14

[2] Nizamoglu S, Gather M C and Yun S H 2013 All-biomaterial laser using vitamin and biopolymers *Adv. Mater.* **25** 5943–7

[3] Ta V D, Caixeiro S, Fernandes F M and Sapienza R 2017 Microsphere Solid-State Biolasers *Adv. Opt. Mater.* **5** 1–6

[4] Lin W J, Liao Y M, Lin H Y, Haider G, Lin S Y, Liao W C, Wei R T, Perumal P, Chang T Y, Tseng C Y, Lo Y S, Lin H M, Shih T W, Hwang J S, Lin T Y and Chen Y F 2018 All-marine based random lasers *Org. Electron. physics, Mater. Appl.* **62** 209–15

[5] Dietrich C P, Steude A, Tropf L, Schubert M, Kronenberg N M, Ostermann K, Höfling S and Gather M C 2016 An exciton-polariton laser based on biologically produced fluorescent protein *Sci. Adv.* **2** 1–7

[6] Gather M C and Yun S H 2014 Bio-optimized energy transfer in densely packed fluorescent protein enables near-maximal luminescence and solid-state lasers *Nat. Commun.*

5 1–8

[7] Caixeiro S, Gaio M, Marelli B, Omenetto F G and Sapienza R 2016 Silk-Based Biocompatible Random Lasing *Adv. Opt. Mater.* **4** 998–1003

[8] Wei Y, Lin X, Wei C, Zhang W, Yan Y and Zhao Y S 2017 Starch-Based Biological Microlasers *ACS Nano* **11** 597–602

[9] Chen Y, Tan X, Sun Q, Chen Q, Wang W and Fan X 2017 Laser-emission imaging of nuclear biomarkers for high-contrast cancer screening and immunodiagnosis *Nat. Biomed. Eng.* **1** 724–35

[10] Polson R C and Vardeny Z V 2004 Random lasing in human tissues *Appl. Phys. Lett.* **85** 1289–91

[11] Wang Y, Duan Z, Qiu Z, Zhang P, Wu J, Dingke A and Xiang T 2017 Random lasing in human tissues embedded with organic dyes for cancer diagnosis *Sci. Rep.* **7** 1–7

[12] Humar M and Yun S H 2015 Intracellular microlasers *Nat. Photonics* **9** 572–6

[13] Schubert M, Steude A, Liehm P, Kronenberg N M, Karl M, Campbell E C, Powis S J and Gather M C 2015 Lasing within Live Cells Containing Intracellular Optical Microresonators for Barcode-Type Cell Tagging and Tracking *Nano Lett.* **15** 5647–52

[14] Kwok S J J, Martino N, Dannenberg P H and Yun S H 2019 Multiplexed laser particles for spatially resolved single-cell analysis *Light Sci. Appl.* **8**

[15] Schubert M, Woolfson L, Barnard I R M, Dorward A M, Casement B, Morton A, Robertson G B, Appleton P L, Miles G B, Tucker C S, Pitt S J and Gather M C 2020 Monitoring contractility in cardiac tissue with cellular resolution using biointegrated microlasers *Nat. Photonics* **14** 452–8

[16] Humar M, Gather M C and Yun S-H 2015 Cellular dye lasers: lasing thresholds and sensing in a planar resonator *Opt. Express* **23** 27865

[17] Gather M C and Yun S H 2011 Lasing from Escherichia coli bacteria genetically programmed to express green fluorescent protein *Opt. Lett.* **36** 3299

[18] Da Silva R R, Dominguez C T, Dos Santos M V., Barbosa-Silva R, Cavicchioli M, Christovan L M, De Melo L S A, Gomes A S L, De Araújo C B and Ribeiro S J L 2013 Silk fibroin biopolymer films as efficient hosts for DFB laser operation *J. Mater. Chem. C* **1** 7181–90

[19] Bakis Dogru I, Melikov R and Nizamoglu S 2018 Biomaterial Disk Lasers by Suppressing the Coffee Ring Effect *ACS Biomater. Sci. Eng.* **4** 4385–90

[20] Nguyen T Van, Pham N Van, Mai H H, Duong D C, Le H H, Sapienza R and Ta V 2019 Protein-based microsphere biolasers fabricated by dehydration *Soft Matter* **15** 9721–6

[21] Venkatakrishnarao D, Mohiddon M A and Chandrasekar R 2017 The Photonic Side of Curcumin: Microsphere Resonators Self-Assembled from Curcumin Derivatives Emitting Visible/Near-Infrared Light *Adv. Opt. Mater.* **5** 1–6

[22] Song Q, Xiao S, Xu Z, Liu J, Sun X, Drachev V, Shalaev V M, Akkus O and Kim Y L 2010 Random lasing in bone tissue. *Opt. Lett.* **35** 1425–7

[23] Ta V D, Saxena D, Caixeiro S and Sapienza R 2020 Flexible and tensile microporous polymer fibers for wavelength-tunable random lasing *Nanoscale* **12** 12357–63

[24] Viola I, Ghofraniha N, Zacheo A, Arima V, Conti C and Gigli G 2013 Random laser emission from a paper-based device *J. Mater. Chem. C* **1** 8128–33

[25] Chang S-W, Liao W-C, Liao Y-M, Lin H-I, Lin H-Y, Lin W-J, Lin S-Y, Perumal P, Haider G, Tai C-T, Shen K-C, Chang C-H, Huang Y-F, Lin T-Y and Chen Y-F 2018 A White Random Laser *Sci. Rep.* **8** 2–11

[26] Kim M, Kim D J, Ha D and Kim T 2016 Cracking-assisted fabrication of nanoscale patterns for micro/nanotechnological applications *Nanoscale* **8** 9461–79

[27] Liu P, Singh S, Guo Y, Wang J J, Xu H, Silien C, Liu N and Ryan K M 2017 Assembling Ordered Nanorod Superstructures and Their Application as Microcavity Lasers *Sci. Rep.* **7** 1–7

[28] Shang Z, Yang M and Deng L 2016 Low-threshold and high intensity random lasing enhanced by MnCl2 *Materials (Basel).* **9** 725

[29] Skjeltorp A T and Meakin P 1988 Fracture in microsphere monolayers studied by experiment and computer simulation *Nature* **335** 424–6

[30] Bakis Dogru I, Melikov R and Nizamoglu S 2018 Biomaterial Disk Lasers by Suppressing the Coffee Ring Effect *ACS Biomater. Sci. Eng.* **4** 4385–90

[31] Ta V D, Nguyen T Van, Pham Q Van and Nguyen T Van 2020 Biocompatible microlasers based on polyvinyl alcohol microspheres *Opt. Commun.* **459** 124925

[32] Tang S K Y, Derda R, Quan Q, Lončar M and Whitesides G M 2011 Continuously tunable microdroplet-laser in a microfluidic channel *Opt. Express* **19** 2204–2015

[33] Nguyen T Van and Ta V D 2020 High-quality factor, biological microsphere and microhemisphere lasers fabricated by a single solution process *Opt. Commun.* **465** 125647

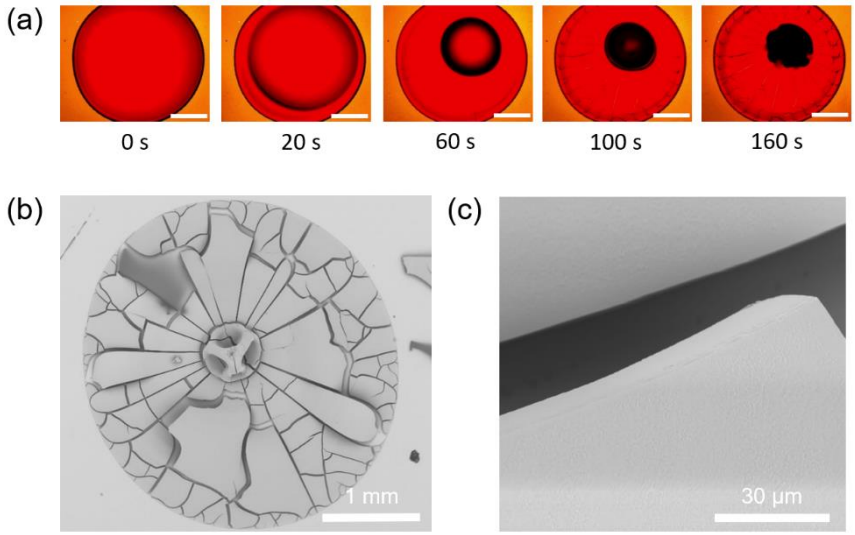

Fig. 1. (a) Optical images of a drying BSA droplet at various time. Cracks start to form at 100 s. The scale bars are 500 µm. (b) SEM image of a dried BSA droplet exhibiting many crack patterns. (c) High magnification SEM image of the edge of a microcrack.

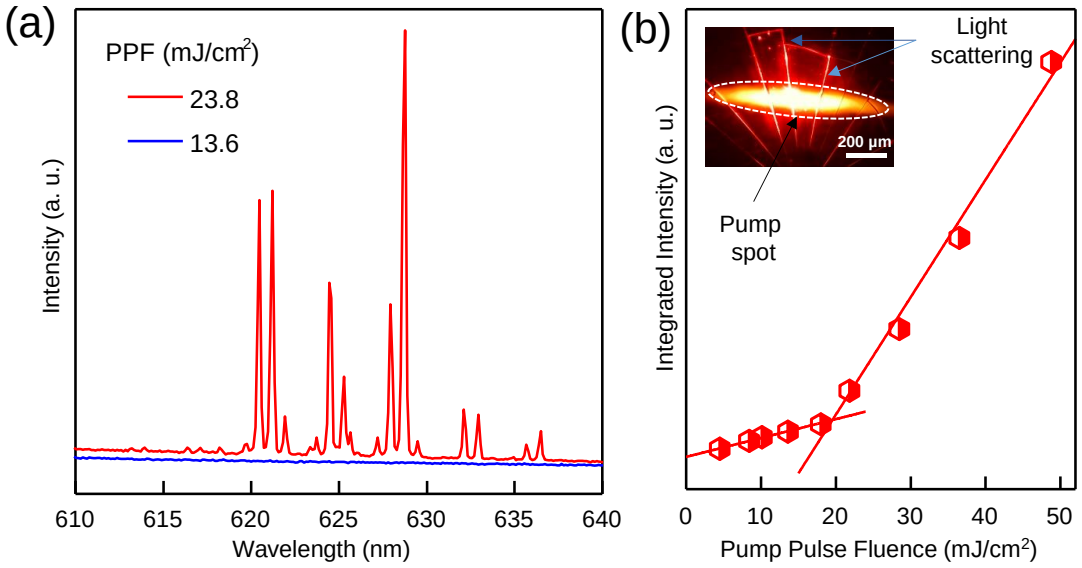

Fig. 2. (a) PL emission spectral of BSA cracks below and above the lasing threshold. (b) Integrated intensity changes as a function of pump pulse fluence.

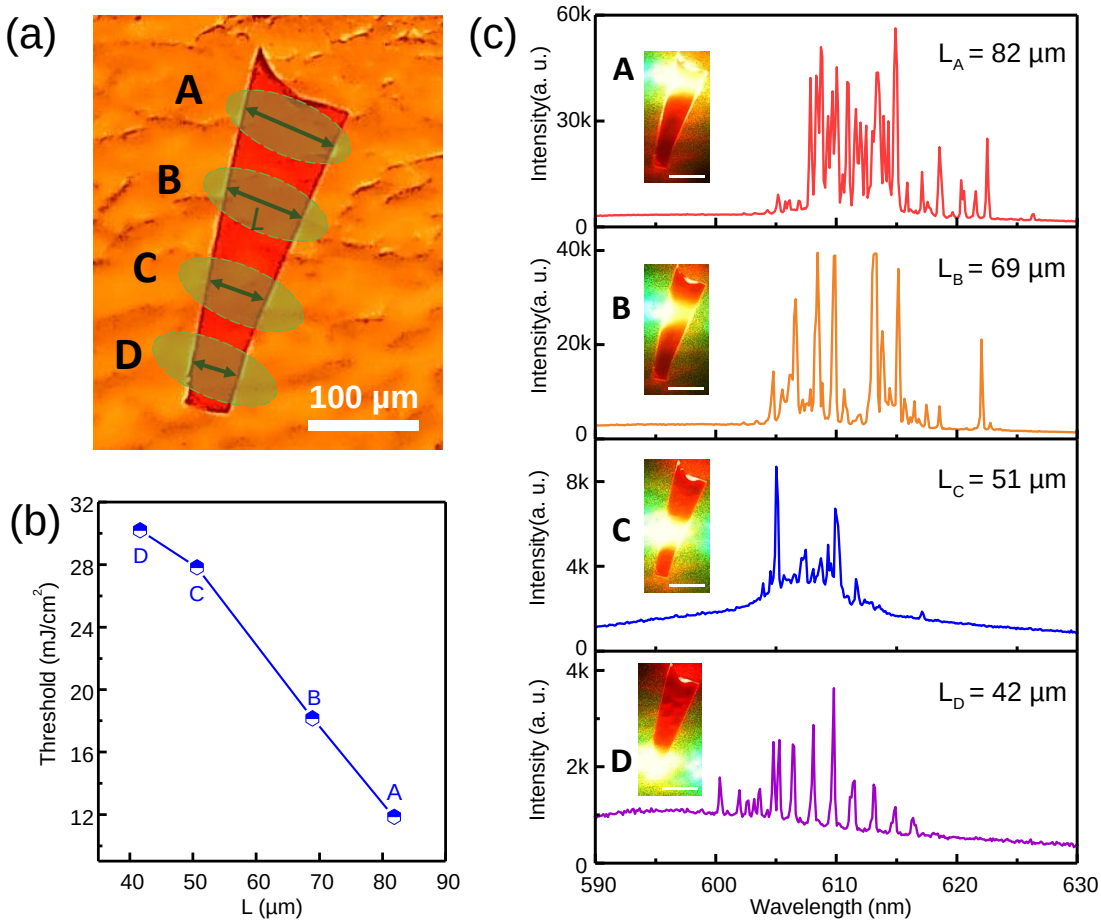

Fig. 3. (a) Optical image of a single BSA crack with denoted pumped positions corresponding to different mean lengths (*L*). (b) Lasing threshold values correspond to the denoted pump positions. (c) Lasing spectrums correspond to different pump positions, the insets present the optical images of different pumped positions of the single BSA crack, the scale bars are 100 μm.

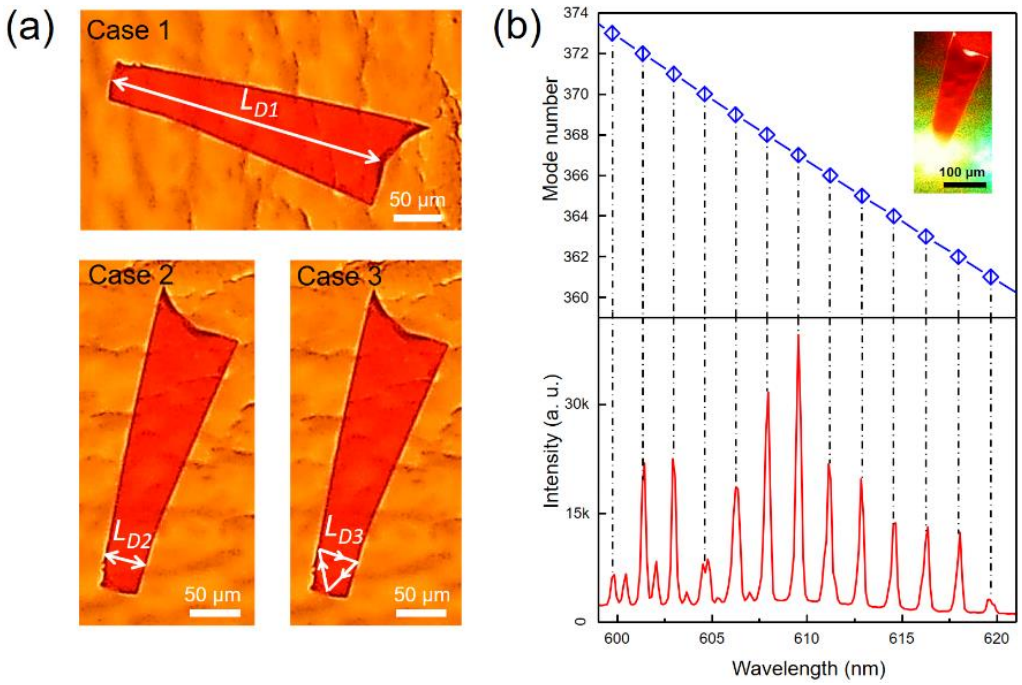

Fig. 4. (a) Three possible cases for optical confinement path at the pumped position D. (b) Numerical calculation of mode number matching with the experimental lasing spectrum at position D.

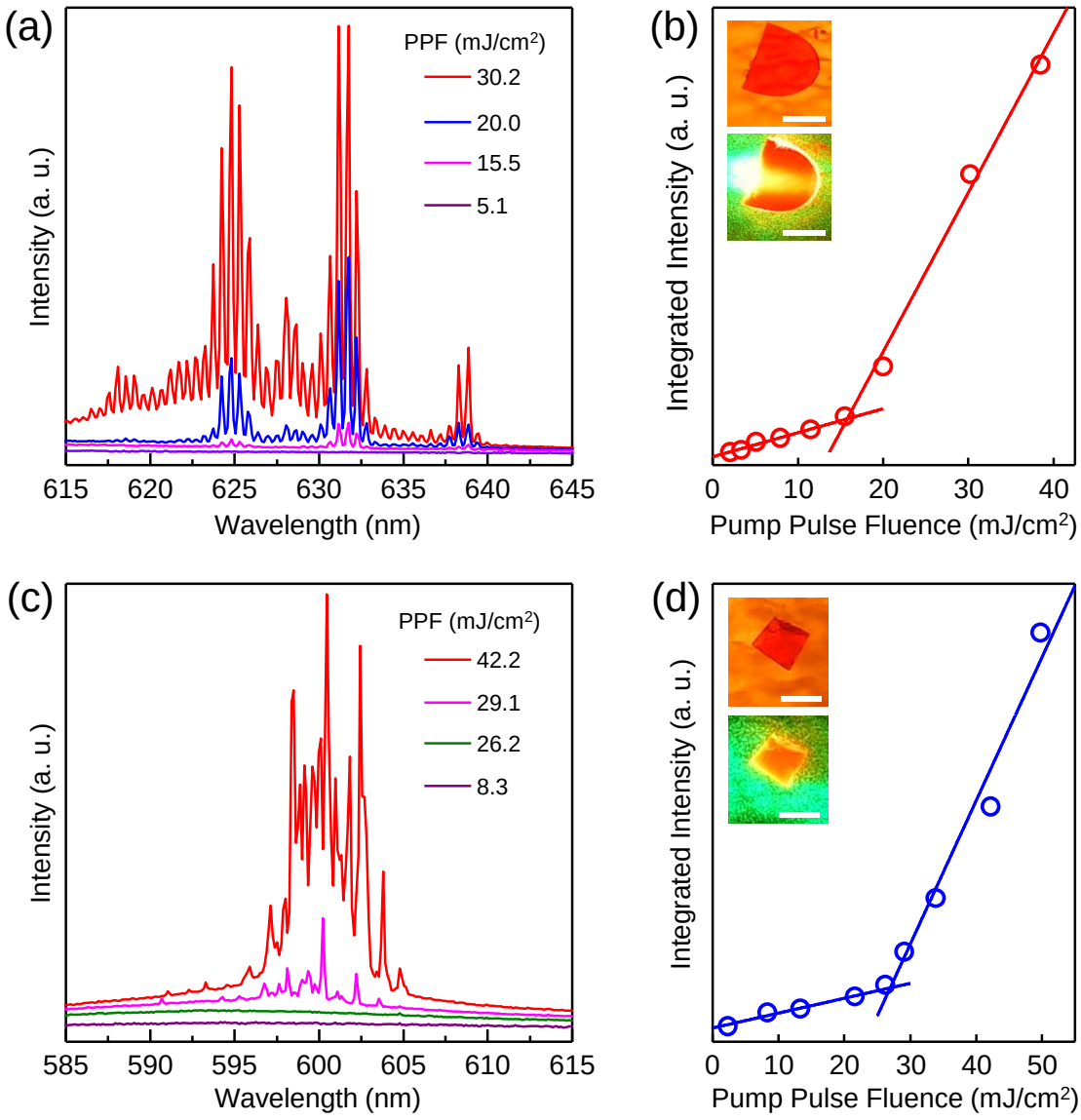

Fig. 5. (a) and (c) PL emission spectra of a 150 μm and a 48 μm BSA crack under increasing pump pulse fluence. (b) and (cd) Corresponding integrated PL intensity of the 150 μm crack laser and the 48 μm crack laser as a function of pump pulse fluence. The insets show the PL and optical image of the laser. Scale bars in (c) are 100 μm and in (d) are 50 μm.